

## THE PULSAR WIND NEBULA OF THE GEMINGA PULSAR

G. G. PAVLOV<sup>1</sup>, D. SANWAL<sup>1</sup>, AND V. E. ZAVLIN<sup>2</sup><sup>1</sup> Dept. of Astronomy & Astrophysics, The Pennsylvania State University, 525 Davey Lab., University Park, PA 16802; pavlov@astro.psu.edu<sup>2</sup> Space Science Laboratory, NASA MSFC SD59, Huntsville, AL 35805*Draft version May 24, 2019*

## ABSTRACT

The superb spatial resolution of *Chandra* has allowed us to detect and resolve a 20''-long tail behind the Geminga pulsar, with a luminosity  $(1.3 \pm 0.2) \times 10^{29}$  ergs s<sup>-1</sup> in the 0.45–8 keV band, for an assumed distance of 200 pc. We also detected an arc-like structure ahead of the pulsar extended perpendicular to the tail, with a factor of 4 lower luminosity. We see no clear evidence of the 2'-long outer tails reported by Caraveo et al. from an *XMM-Newton* observation. The tail we detected could be either a pulsar jet, possibly confined by a toroidal magnetic field of  $\sim 100 \mu\text{G}$ , or it can be associated with the shocked relativistic wind behind the supersonically moving pulsar confined by the ram pressure of the oncoming interstellar medium.

*Subject headings:* pulsars: individual (Geminga) – stars: neutron — stars: winds, outflows

## 1. INTRODUCTION

Most of the energy loss from pulsars occurs in the form of a relativistic pulsar wind (PW). The PW shocks in the ambient medium forming a pulsar-wind nebula (PWN) which emits synchrotron radiation (Rees & Gunn 1974). An isotropic outflow from a stationary pulsar in a uniform medium forms a spherical termination shock (TS) at a radius  $R_s \simeq (\dot{E}/4\pi c p_{\text{amb}})^{1/2}$ , where  $\dot{E}$  is the pulsar's spin-down power and  $p_{\text{amb}}$  is the ambient pressure. For a pulsar moving at a speed  $v$  with respect to the medium, the TS shape is distorted by the ram pressure,  $p_{\text{ram}} = \rho_{\text{amb}} v^2$ . At supersonic speeds, when the ram pressure exceeds the ambient pressure, the TS of an isotropic PW acquires a bullet-like shape (Bucciantini, Amato, & Del Zanna 2005 [hereafter B05], and references therein) with a distance  $R_h \simeq (\dot{E}/4\pi c p_{\text{ram}})^{1/2}$  between the pulsar and the bullet head. The shocked PW is confined between the TS and the contact discontinuity (CD) surface which separates the shocked PW from the shocked ambient medium between the CD and the forward bow shock (FBS). The shape of the shocks and the overall appearance of the PWN depend on the interplay of  $\dot{E}$ ,  $p_{\text{amb}}$ ,  $\rho_{\text{amb}}$ , and  $v$ . Thus, PWNe produced by fast-moving pulsars provide an important diagnostic tool for studying the PW, the ambient medium, and the space velocity of the pulsar.

X-ray PWNe have been observed around about 30 pulsars. High-resolution observations with *Chandra* show that the PWN structure is never a simple spherical shell. In particular, young PWNe (e.g., the Crab and Vela PWNe; Weisskopf et al. 2000; Pavlov et al. 2003) are often approximately axially symmetric, with jets along the symmetry axis (which apparently coincides with the pulsar's spin axis in well-studied cases) and a torus-like structure around the axis (an equatorial PW outflow). There are some X-ray PWNe whose cometary shape is clearly caused by the pulsar motion. Some of them (e.g., the Mouse PWN, powered by the young PSR J1747–2958; Gaensler

et al. 2004) are confined within a bow-like boundary, but they do not show a shell structure, in contrast to the sharp H<sub>α</sub> “bows” emitted by the shocked ambient gas at FBSs produced by some pulsars. *Chandra* observations of the pulsars B1757–24 (Kaspi et al. 2001), B1957+20 (Stappers et al. 2003), J1509–5859, and J1809–1917 (Sanwal et al. 2006) revealed linear structures (of lengths  $\sim 0.05$ –0.5 pc) which look like “trails” behind moving pulsars. An exceptionally long ( $\sim 1.6$  pc) trail was found behind PSR B1929+10 by Wang, Li, & Begelman (1993). The origin of these trails has not been firmly established (see §4).

An intriguing PWN structure has been recently reported by Caraveo et al. (2003; hereafter C03) from the data collected in first *XMM-Newton* observation of the middle-aged pulsar Geminga ( $\tau = 340$  kyr,  $\dot{E} = 3.3 \times 10^{34}$  ergs s<sup>-1</sup>). They found two 2'-long tails behind the pulsar, with a luminosity of  $\sim 10^{29}$  ergs s<sup>-1</sup> in the 0.3–5 keV band. They suggested that these are the tails of a bow shock generated by pulsar's motion and predicted the head of the bow-shock to be at an angular distance of 20''–30'' ahead of the pulsar. In this Letter, we present the results of our high-resolution *Chandra* observation of the Geminga PWN in the vicinity of the pulsar<sup>1</sup> and confront them with the results of the *XMM-Newton* observation and theoretical models.

## 2. OBSERVATIONS AND DATA REDUCTION

*Chandra* observed Geminga on 2004 February 7 for 19.9 ks (18.8 ks good exposure time) with the ACIS detector. The pulsar was positioned on the ACIS-S3 chip with a standard Y offset of  $-0'.33$ . A 1/8 subarray mode (frame time of 0.7 seconds) was used to mitigate the CCD pileup in the pulsar image. We used CIAO 3.2.2 tools (CALDB 3.1.0) for the analysis, starting from the level 1 event files to correct for charge transfer inefficiency (CTI) using the software *ACISCTICorrector.1.37*<sup>2</sup> (see Townsley et al. 2000). We applied the standard grade filtering (retaining grades

<sup>1</sup>Preliminary results have been presented by Sanwal, Pavlov, & Zavlin (2004).<sup>2</sup>available at <http://www.astro.psu.edu/users/townsley/cti/>

02346) and removed events with energy  $> 8$  keV to reduce the background. Since no events with  $E < 0.45$  keV were detected on the S3 chip, we use the 0.45–8 keV band for further analysis.

We also reanalyzed the *XMM-Newton* EPIC data taken on 2002 April 4–5 (103 ks exposure, with EPIC-PN in Small Window mode and EPIC-MOS in Prime Full Window mode). We used SAS v.6.1 to reprocess and analyze the data. The effective exposure times, after removing the periods of high background, are about 68 ks for EPIC-PN, and about 82 ks for MOS1 and MOS2. A detailed analysis of the MOS data was presented by C03. We will supplement those results with the analysis of the EPIC-PN data.

### 3. OBSERVATIONAL RESULTS

#### 3.1. *XMM-Newton EPIC-PN* Results

The raw MOS and PN images do not show extended structures in the vicinity of Geminga. However, after some experimenting with image smoothing, two elongated patchy structures become visible, stretched in the direction opposite to the pulsar's proper motion (we will call them *outer tails* to distinguish from the short inner tail discovered with *Chandra*; see below). Figure 1 (left panel) shows these structures, seen up to about 3' from the pulsar ( $\sim 0.17d_{200}$  pc, where  $d_{200}$  is the distance<sup>3</sup> scaled to 200 pc) in the smoothed PN image, similar to those in smoothed MOS images. The average image brightness of these tails in the PN image (0.3–8 keV band, extraction box of  $40'' \times 80''$  for each tail) is about  $1 \times 10^{-6}$  counts s $^{-1}$  arcsec $^{-2}$ . Spectral analysis of the tail emission is hindered by the small number of counts and nonuniform background. Using the absorbed power-law spectral model with the parameters estimated by C03 from the MOS data (photon index  $\Gamma = 1.6$ , hydrogen column density  $N_{\text{H}} = 1.1 \times 10^{20}$  cm $^{-2}$ ), we obtain the surface brightness (intensity) of the outer tails  $I_{\text{outer}} \sim 3 \times 10^{-18}$  ergs cm $^{-2}$  s $^{-1}$  arcsec $^{-2}$ , and the total unabsorbed flux  $F_{\text{outer}} \sim 2 \times 10^{-14}$  ergs cm $^{-2}$  s $^{-1}$ . This gives the luminosity  $L_{\text{outer}} \sim 1 \times 10^{29} d_{200}^2$  ergs s $^{-1}$   $\approx 3 \times 10^{-6} \dot{E} d_{200}^2$ , in agreement with the value reported by C03.

Since C03 used the Wilkin (1996) analytical bow-shock model<sup>4</sup> to describe the shape of the tails in the MOS images, we fit the PN image with the same model. In agreement with C03, the best-fit model (for inclination angle  $i = 90^\circ$  between the line of sight and the pulsar velocity) gives a stand-off distance of about 20'', hidden in the bright pulsar image broadened by the wide *XMM-Newton* PSF (Fig. 1, left panel). Thus, the PN data show the properties of the putative tails consistent with those derived by C03 from the MOS data. It, however, remains unclear whether the tails are real or they are simply a coincidental superposition of faint background objects (such as the point source marked 'X' in the left panel of Fig. 1 and in Fig. 2), which mimics the patchy tail-like structures in the smoothed image.

#### 3.2. *Chandra ACIS* Results

The excellent spatial resolution of *Chandra* provides a close-up view in the vicinity of Geminga, shown in Figure 1 (right panel). The *Chandra* image shows no emission

20'' ahead of the pulsar, where the head of the bow-shock would be expected from the extrapolation of the putative outer tails. Instead, we see some diffuse emission at a distance of 5''–7'', whose shape resembles an *arc* extended perpendicular to the proper motion direction. Since the pulsar count rate is only 0.07 counts/frame, this structure is not expected to be caused by pileup in the pulsar image. The  $15 \pm 5$  background-subtracted counts (extracted from a  $5'' \times 16''$  ellipse shown in Fig. 2) correspond to an average image brightness of about  $1 \times 10^{-5}$  counts s $^{-1}$  arcsec $^{-2}$ . Assuming a power-law spectrum with  $\Gamma = 1.6$ , the average intensity of this region is  $I_{\text{arc}} \sim 1 \times 10^{-16}$  ergs cm $^{-2}$  s $^{-1}$  arcsec $^{-2}$ , about 30 times brighter than the tails seen with EPIC. The X-ray luminosity of this structure is  $L_{\text{arc}} \sim 3 \times 10^{28} d_{200}^2$  ergs s $^{-1}$ .

Figure 2 shows a  $1.0'' \times 2.5''$  adaptively smoothed ACIS-S3 image with overplotted Wilkin (1996) bow-shock models for  $i = 90^\circ$ . We see no emission along the 20'' curve in the ACIS image, even at the locations where the tails seen with EPIC are outside the bright pulsar image (e.g.,  $\sim 1'$  south of the pulsar). There is some hint of brightness enhancement between the 20'' and 10'' curves ( $23 \pm 15$  background-subtracted counts in the  $25'' \times 60''$  box in Fig. 2), corresponding to an intensity about twice higher than that in the tails observed with EPIC, but it is not statistically significant. Thus, we see no evidence of the outer tails in the ACIS image, but we cannot conclusively reject their presence because the *Chandra* exposure was too short.

The most striking feature in the ACIS image is a  $\sim 5''$ -wide "axial tail", seen up to 25'' ( $7.5 \times 10^{16} d_{200}$  cm) from the pulsar in the direction opposite to the pulsar's proper motion. The tail is apparently detached from the pulsar by 5''–6''; its brightness is maximal at  $\sim 8''$ , and it fades with increasing distance from the pulsar. The average image brightness in the  $6'' \times 12''$  box (see Fig. 2), which contains  $37.1 \pm 6.3$  background-subtracted counts, is  $2.7 \times 10^{-5}$  counts s $^{-1}$  arcsec $^{-2}$ . Although the small number of counts precludes detailed spectral analysis, its spectrum is consistent with a power-law with a photon index  $\Gamma = 1.0 \pm 0.4$  (the errors correspond to the 90% confidence level for one interesting parameter), somewhat harder than the spectrum of the outer tails. The intensity of the tail (in the  $6'' \times 12''$  box),  $I_{\text{axial}} = 3 \times 10^{-16}$  ergs cm $^{-2}$  s $^{-1}$  arcsec $^{-2}$  in the 0.45–8 keV band, is about 2 orders of magnitude higher than that of the tails seen with EPIC. Its luminosity,  $L_{\text{axial}} = (1.3 \pm 0.2) \times 10^{29} d_{200}^2$  ergs s $^{-1}$  (measured from  $49.1 \pm 7.3$  background-subtracted counts in a  $6'' \times 20''$  box detached by 6'' from the pulsar), is close to the total luminosity of the putative outer tails.

### 4. DISCUSSION

If the tails in the EPIC images are real, the Geminga PWN is truly unique: a bow-shock-like structure with long outer tails *and* a short axial tail behind the pulsar have never been seen before. Even if the outer tails are an artifact, the axial tail and the arc detected with ACIS are by no means common and deserve a detailed investigation.

Before discussing possible interpretations of the observed structures, we note that the proper motion of

<sup>3</sup>The distance to Geminga is unknown (see Kargaltsev et al. 2005), but  $d \sim 200$  pc is a reasonable estimate.

<sup>4</sup>Rigorously speaking, such a model is inapplicable to the tails of an X-ray PWN (see, e.g., B05).

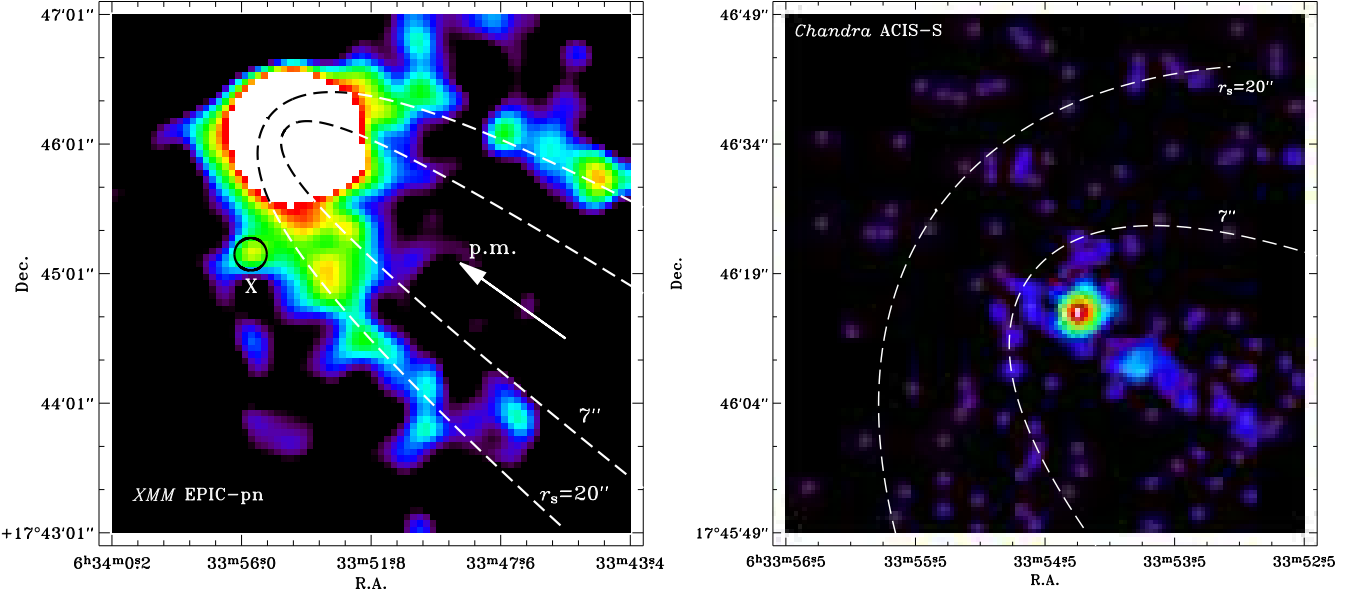


FIG. 1.— *Left*: Smoothed XMM-Newton EPIC-PN image of a  $4' \times 4'$  region around Geminga showing the two outer tails. The shape of the tails is fit by the Wilkin (1996) model with a stand-off distance of  $20''$ . The arrow shows the direction of pulsar's proper motion. The black circle indicates the position of the point source X resolved in the *Chandra* image (Fig. 2). *Right*: Smoothed *Chandra* ACIS-S3 image of a  $1' \times 1'$  region around Geminga showing an extended emission at  $5''$ – $7''$  ahead of the pulsar (the arc) and a  $20''$ -long axial tail. No emission is seen at  $20''$  ahead of the pulsar.

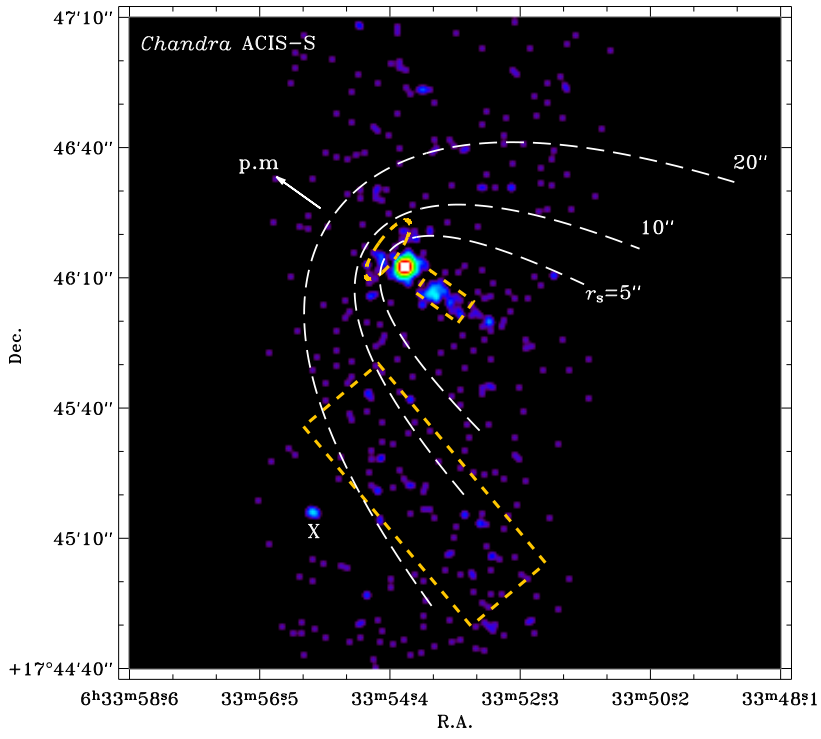


FIG. 2.— Smoothed *Chandra* ACIS-S3 image of a  $1'0 \times 2'.5$  region around Geminga, with three Wilkin (1996) bow-shock models plotted to guide the eye. 'X' marks a point source near the putative southern outer tail of the EPIC image. The rectangular region between the  $10''$  and  $20''$  bow-shock models was used to examine an apparent brightness enhancement at the site close to the southern outer tail.

Geminga,  $0''.17 \text{ yr}^{-1}$ , implies a pulsar speed,  $v = 160 \tilde{d} \text{ km s}^{-1}$ , where  $\tilde{d} = d_{200} / \sin i$ . For a reasonable distance, it exceeds a typical sound speed in the interstellar medium (ISM),  $c_s = 15(\mu/0.6)^{-1/2}T_4^{1/2} \text{ km s}^{-1}$ , where  $\mu$  and  $T = 10^4 T_4 \text{ K}$  are the molecular weight and tem-

perature. Assuming that the speed of a possible ISM flow at the location of Geminga is much lower than  $v$ , the ram pressure due to the pulsar motion in the ISM is  $p_{\text{ram}} = 4.3 \times 10^{-10} n \tilde{d}^2 \text{ ergs cm}^{-3}$ , where  $n$  is the ISM density in atomic mass units per  $\text{cm}^3$ . This gives an estimate

$R_h = 1.4 \times 10^{16} n^{-1/2} \tilde{d}^{-1}$  cm for the stand-off distance of the TS head, which translates into the projected angular distance  $\mathcal{R}_h = 4''.8 n^{-1/2} \tilde{d}^{-2}$ . Thus, one can expect that Geminga is accompanied by a bow-shock PWN, with a characteristic size comparable to the sizes of the structures observed with *Chandra* and, possibly, *XMM-Newton*. We will discuss possible interpretations of the whole PWN, starting each from an assumption on the nature of the axial tail, the brightest and most firmly established feature of the PWN.

#### 4.1. The axial tail is a shocked pulsar wind?

The axial tail could be interpreted as synchrotron emission from the shocked PW collimated by the ram pressure. According to the simulations by B05, who assumed an *isotropic PW*, the TS has a bullet-like shape. For large Mach numbers,  $c_s/v$ , and small values of the magnetization parameter  $\sigma$  of the pre-shock PW, the bullet's cylindrical radius is  $r_{TS} \sim R_h$ , and the distance of its back surface from the pulsar is  $R_b \sim 6R_h$ . The shocked PW outside the TS is confined inside the CD surface which has a cylindrical shape behind the TS, with a radius  $r_{CD} \sim 4R_h$ . The collimated PW flows with subrelativistic velocities: 0.1–0.3  $c$  in the inner channel ( $r \lesssim r_{TS}$ ) and up to 0.8–0.9  $c$  in the outer channel ( $r_{TS} \lesssim r \lesssim r_{CD}$ ).

First, one can speculate that the axial tail is the CD-confined cylindrical tube behind the TS, which implies a CD radius of  $\sim 3''$  and  $\mathcal{R}_h \sim 0''.7$ . In this interpretation, one should expect brightest emission from the shocked PW at  $\lesssim 1''$  ahead of the pulsar, hidden within the pulsar image. The actually observed emission  $\sim 5''$ – $7''$  ahead of the pulsar (the arc) is not explained by this model. Being well outside the CD, the two outer tails cannot be associated with a shocked PW. One might speculate that they are produced by the shocked ISM heated to X-ray temperatures, but the pulsar's speed is too low to support this speculation, and thermal models with reasonable temperatures do not fit the tails spectrum. Overall, given the problems with explaining the observed PWN structure, this interpretation of the axial tail is hardly viable.

Second, one could assume that the axial tail is associated with the shocked PW “sheath” immediately outside the TS, similar to the interpretations of the tail behind PSR B1757–24 by Gvaramadze (2002) and the “tongue” of the X-ray Mouse PWN by Gaensler et al. (2004). The two outer tails might be associated with emission from a shell immediately inside the CD surface, where the magnetic field is compressed (see B05) and hence the synchrotron emissivity could be enhanced<sup>5</sup>. In this interpretation, the outer tails should be parallel to the direction of pulsar motion, which is crudely in agreement with observations, but their distance from the PWN axis,  $\sim 60''$ – $70''$ , implies  $\mathcal{R}_h \sim 15''$ – $18''$ , where no emission is seen in the *Chandra* image. On the other hand, the width of the axial tail suggests  $\mathcal{R}_b \sim 15''$ , somewhat shorter than the observed tail's length, and  $\mathcal{R}_h \sim 2''.5$ , smaller than the distance to the arc in the *Chandra* image. Moreover, the arc is, on average, a factor of 4 dimmer than the tail, and its extent perpendicular to the pulsar's proper motion is possibly a factor of 3–5 larger than the tail's width. Therefore, we are forced to assume that the TS head is unresolved from the pulsar, while

the arc might be a CD head at a distance  $\sim 2.8R_h$  from the pulsar, larger than  $\sim 1.3R_h$  in the B05 simulations. The corresponding ratio  $r_{CD}/R_h \sim 25$ – $30$  is much larger than  $\sim 4$  in the B05 simulations. These discrepancies could be caused by *anisotropy of the pulsar outflow*, neglected by B05. For instance, if the outflow is mostly equatorial (assuming the pulsar's rotation axis aligned with its space velocity), the flattened TS head should be closer to the pulsar than in the isotropic case.

We should also mention that this interpretation implies a rather large tail's length,  $l_{tail} \sim v_{flow}\tau_{syn}$ , where  $v_{flow}$  is the flow velocity and  $\tau_{syn} = 5.1 \times 10^8 \gamma^{-1} B^{-2}$  s is the synchrotron cooling time. The magnetic field just downstream of the TS back boundary can be estimated, for  $\sigma \ll 1$ , as  $B_b \simeq 3(\dot{E}\sigma/R_b^2 c)^{1/2} \simeq 70(\mathcal{R}_b/15'')^{-1} \tilde{d}^{-1} \sigma^{1/2} \mu G$  (cf. Kennel & Coroniti 1984). The synchrotron photons with maximum observed energies  $E \approx 8$  keV are emitted by electrons with a Lorentz factor  $\gamma \sim 1.3 \times 10^8 (E/8\text{ keV})^{1/2} (B/100 \mu G)^{-1/2} \sim 1.5 \times 10^8 (E/8\text{ keV})^{1/2} \tilde{d}^{1/2} (\mathcal{R}_b/15'')^{1/2} \sigma^{-1/4}$ . This gives  $l_{tail} \sim 4 \times 10^{18} (v_{flow}/0.2c) (E/8\text{ keV})^{-1/2} \tilde{d}^{3/2} (\mathcal{R}_b/15'')^{3/2} \sigma^{-3/4}$  cm, which exceeds the observed length by two orders of magnitude even at lowest  $v_{flow} \sim 0.1c$  in the inner channel behind the TS, as found by B05.

Thus, we cannot rule out that the axial tail is the emission from the freshly shocked PW immediately outside the TS while the outer tails mark the CD surface. This interpretation, however, is not quantitatively consistent with the simulations based on the assumption of isotropy of the pre-shock PW.

#### 4.2. The axial tail is a pulsar jet?

Another explanation of the axial tail is that it is a *jet* emanating from the pulsar magnetosphere along the spin axis aligned with the pulsar's motion. The fact that only one jet is seen is not uncommon (PSR B1706–44 is a vivid example; Ng & Romani 2004), and it can be explained by Doppler boosting (the approaching jet is brighter than the receding one) and/or by an intrinsic anisotropy of the polar outflows, or it may be caused by destruction of the forward jet by the ISM ram pressure. The Geminga's axial tail can be analogous to the southwest jet (“inner counterjet” in Pavlov et al. 2003) of the Vela PWN, which is about twice brighter than the northeast jet in the direction of pulsar's motion. The projected length of Vela's southwest jet,  $5 \times 10^{16} d_{300}$  cm, is close to that of the Geminga's axial tail, the spectra of both structures are very hard, and the ratios of their X-ray luminosities to the pulsar spindown powers are not very different:  $L_X/\dot{E} \sim 3.6 \times 10^{-6} d_{200}^2$  for the Geminga's tail and  $\sim 0.6 \times 10^{-6} d_{300}^2$  for the Vela's southwest jet.

If the jet is confined by its own magnetic field, a lower limit on the field can be estimated from the requirement that the electron Larmor radius is smaller than the jet radius,  $r_{jet} \sim 0.75 \times 10^{16} d_{200}$  cm, which gives  $B > 90(E_M/8\text{ keV})^{1/3} d_{200}^{-2/3} \mu G$ , where  $E_M$  is the maximum energy of the X-ray power-law spectrum (cf. Pavlov et al. 2003). It corresponds to the energy injection rate,  $\dot{W} = (B^2/8\pi)(1+k)v_{jet}\pi r_{jet}^2 > 7.8 \times 10^{32} (1+k)(\beta/0.5)(E_M/8\text{ keV})^{2/3} d_{200}^{2/3}$  ergs  $\text{s}^{-1}$ , where  $v_{jet} = \beta c$  is

<sup>5</sup>Note, however, that the simulation of intensity by B05 do not show bright shell-like structures.

the bulk flow velocity in the jet, and  $k$  is the ratio of particle and magnetic energy densities. Even this lower limit on  $\dot{W}$  is a substantial fraction of the spindown power for a mildly relativistic  $v_{\text{jet}}$  expected for a pulsar jet (e.g.,  $\dot{W} \sim 0.05\dot{E}$  for  $k = 1$  and  $\beta = 0.5$ ), which means that the magnetic field cannot strongly exceed the above lower limit. At such magnetic fields one would expect a jet length  $l_{\text{jet}} \sim v_{\text{jet}}\tau_{\text{syn}} \sim 2 \times 10^{18}(\beta/0.5)(B/100\mu\text{G})^{-3/2}(E_{\text{M}}/8\text{keV})^{-1/2}$  cm, much larger than the observed  $\sim 7 \times 10^{16}\tilde{d}$  cm. Therefore, we have to assume that the jet is destroyed or becomes uncollimated well before it loses its internal energy to radiation.

If the axial tail is a pulsar jet, the outer tails could mark an equatorial outflow bent by the ram pressure. We are unaware of theoretical models for PWNe which include both the PW anisotropy and the ram pressure effects. We, however, expect that the equatorial PW component (which would produce a torus beyond a TS ring around a slowly-moving pulsar) would form a relatively thin shell between the TS and CD surface behind the pulsar, filled by a relativistic plasma with a subrelativistic bulk flow velocity. If the outer tails turn out to be an artifact, we would suggest that most of the PW flows out of the magnetosphere

along the spin axis while the equatorial PW component is unusually weak in Geminga (perhaps because of a small angle between the magnetic and spin axes). The arc ahead of the pulsar could be a head of the bent equatorial outflow or remnants of a forward jet crushed by the ISM ram pressure.

To summarize, the *Chandra* observation has conclusively shown the presence of PWN elements around the Geminga pulsar. With the sparse statistics of the *Chandra* data and the low spatial resolution of the *XMM-Newton* data, we cannot establish the nature of the extended emission unambiguously. However, it seems certain that the observed PWN structure implies that the Geminga's PW is intrinsically anisotropic. Much deeper observations with high spatial resolution and modeling of magnetized anisotropic winds from fast-moving pulsars are needed to clarify the nature of this intriguing PWN.

We thank Niccolò Bucciantini for useful discussions. Support for this work was provided through Chandra Award Number GO4-5083X and NASA grant NAG5-10865. The work of V.E.Z. is supported by a NRC Research Associateship Award at NASA MSFC.

#### REFERENCES

Bucciantini, N., Amato, E., & Del Zanna, L. 2005, *A&A*, 434, 189 (B05)  
 Caraveo, P. A., Bignami, G. F., DeLuca, A. et al. 2003, *Science*, 301, 1345 (C03)  
 Gaensler, B. M., et al. 2004, *ApJ*, 616, 383  
 Gvaramadze, V. 2004, *A&A*, 415, 1073  
 Kargaltsev, O. Y., Pavlov, G. G., Zavlin, V. E., & Romani, R. W. 2005, *ApJ*, 625, 327  
 Kaspi, V. M., Gotthelf, E. V., Gaensler, B. M., & Lyutikov, M. 2001, *ApJ*, 562, L163  
 Kennel, C. F., & Coroniti, F. V. 1984, *ApJ*, 283, 694  
 Ng & Romani 2004, *ApJ*, 601, 479  
 Pavlov, G. G., Teter, M. A., Kargaltsev, O., & Sanwal, D. 2003, *ApJ*, 591, 115  
 Rees, M.J., & Gunn, J.E., 1974, *MNRAS*, 164, 1  
 Sanwal, D., Pavlov, G. G., & Zavlin, V. E. 2004, *AAS HEAD meeting*, #8, #11.06  
 Sanwal, D., et al. 2006, *ApJ*, in preparation  
 Stappers, B. W., Gaensler, B. M., Kaspi, V. M., van der Klis, M. & Lewin, W. H. G. 2003, *Science*, 299, 1372  
 Townsley, L. K., Broos, P. S., Garmire, G. P., & Nousek, J. A. 2000, *ApJ*, 534, L139  
 Wang, Q. D., Li, Z.-Y., & Begelman, M. C. 1993, *Nature*, 364, 127  
 Weisskopf, M. C., et al. 2000, *ApJ*, 536, L81  
 Wilkin, F. P. 1996, *ApJ*, 459, L31